Composites: Part A 100 (2017) 361–370

Contents lists available at ScienceDirect

Composites: Part A

journal homepage: www.elsevier.com/locate/compositesa

Robust sacrificial polymer templates for 3D interconnected microvasculature in fiber-reinforced composites

J.F. Patrick [a], B.P. Krull [a,b], M. Garg [a,b], C.L. Mangun [c], J.S. Moore [a,d], N.R. Sottos [a,b,*], S.R. White [a,e,*]

[a] Beckman Institute for Advanced Science and Technology, University of Illinois at Urbana-Champaign, Urbana, IL 61801, USA
[b] Department of Materials Science and Engineering, University of Illinois at Urbana-Champaign, Urbana, IL 61801, USA
[c] CU Aerospace LLC, Champaign, IL 61820, USA
[d] Department of Chemistry, University of Illinois at Urbana-Champaign, Urbana, IL 61801, USA
[e] Department of Aerospace Engineering, University of Illinois at Urbana-Champaign, Urbana, IL 61801, USA

ARTICLE INFO

Article history:
Received 20 January 2017
Received in revised form 10 May 2017
Accepted 18 May 2017
Available online 30 May 2017

Keywords:
A. Multifunctional composites
B. Microstructures
E. 3-D printing
Weaving

ABSTRACT

A promising pathway for multifunctionality in fiber-composites is to mimic biological vasculature that enables living organisms with concerted homeostatic functions. In this paper, newfound material and processing advancements in vaporization of sacrificial components (VaSC), a technique for creating inverse replica architectures via thermal depolymerization of a sacrificial template, are established for enhanced vascular composites manufacturing. Sacrificial poly(lactic acid) with improved distribution of catalytic micro-particles is extruded into fibers for automated weaving and filament feedstock for 3-D printing. Fiber drawing after extrusion improves mechanical robustness for high-fidelity, composite preform weaving. Joining one-dimensional (1D) interwoven fibers with printed sacrificial (2D) templates affords three-dimensional (3D) interconnected networks in a fiber-composite laminate that inherits damage-tolerant features found in natural vasculatures. In addition to providing a conduit for enhanced functionality, the sacrificial templating techniques are compatible with current composites manufacturing processes, materials, and equipment.

1. Introduction

In biological systems, fluid transport through internal vasculature enables a variety of metabolic and homeostatic functions including respiration, circulation, thermal regulation, and self-repair. Natural, load-bearing materials such as bone and wood rely on nutrient exchange through vascular networks to achieve cellular proliferation (growth) and tissue regeneration (repair). Fiber-reinforced composites (FRC) possess comparable structural characteristics to natural counterparts, but lack the dynamic functionality enabled by hierarchical vasculature. The fabrication of vascular architectures (Fig. 1) with sacrificial precursors that can also survive the stringent manufacturing requirements of the host material has been a long standing challenge.

Direct-write assembly (DWA) [1,2] of wax-based fugitive inks produces intricate, 3D interconnected vascular templates that can be melted and removed from solid polymer after liquid monomer infusion and solidification [3–7]. These sacrificial scaffolds however, are too delicate to survive FRC manufacturing under elevated temperatures and/or compaction pressure during cure. Several research groups have created 1D microchannels (Fig. 1a) within FRC for self-healing and sensing applications by embedding hollow glass fibers [8–12], manual extraction of silicone tubes [13,14] or steel wires coated with chemical release agent [15–20], or "lost-wax" removal of melted solder wires via heat and vacuum [21–23]. Yet, these approaches lack the capability to create three-dimensional, interconnected networks - a critical requirement for replicating biologically inspired architectures and functions.

The vaporization of sacrificial components (VaSC) process [24–28] has proven to be a robust method for creating multi-dimensional microvascular networks within FRC. Early VaSC demonstrations [24,25] relied on solvent swelling of poly(lactic acid) (PLA) fibers to locally incorporate tin (II) oxalate (SnOx) catalyst particles that facilitate lower temperature depolymerization through bond cleavage in the polymer backbone. More recent studies [28,29] have incorporated catalysts by solvent- or melt-blending techniques to improve homogeneity within the sacrificial

* Corresponding authors at: 3365, Beckman Institute, 405 North Mathews Avenue, Urbana, IL 61801, USA (N.R. Sottos). 3361, Beckman Institute, 405 North Mathews Avenue, Urbana, IL 61801, USA (S.R. White).
E-mail addresses: n-sottos@illinois.edu (N.R. Sottos), swhite@illinois.edu (S.R. White).

http://dx.doi.org/10.1016/j.compositesa.2017.05.022
1359-835X/

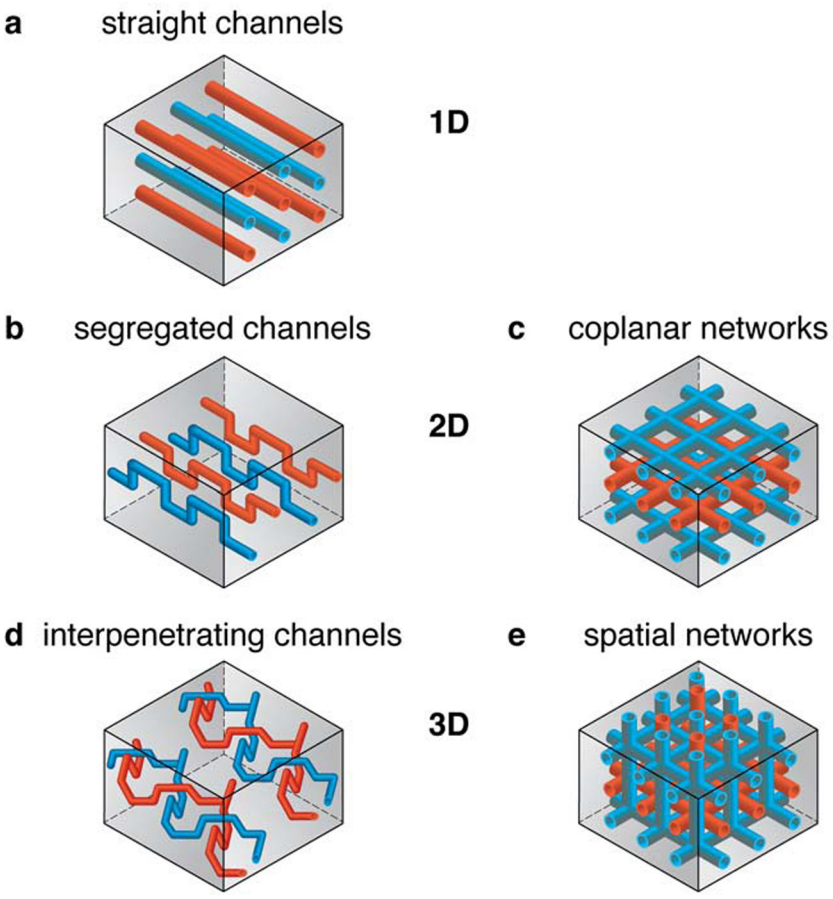

Fig. 1. Vascular hierarchy. (a) One-dimensional (1D) straight channels; (b) Two-dimensional (2D) segregated channels; (c) 2D coplanar interconnected networks; (d) Three-dimensional (3D) interpenetrating channels; (e) 3D spatial interconnected networks.

polymer. DWA has been used to print sacrificial PLA scaffolds via solvent-casting which were subsequently removed from cured epoxy to reveal isolated, spiral microchannels [29]. Fused deposition modeling (FDM) has also been adapted to create multi-dimensional sacrificial PLA templates that were subsequently evacuated from neat epoxy [28]. Three-dimensional, interpenetrating vasculature (Fig. 1d) has been constructed in FRC laminates by VaSC of interwoven sacrificial PLA fibers, and were shown to improve *in situ* mixing of liquid healing agents [30]. However, the resulting microchannels lacked interconnectivity and pathway redundancy, rendering them prone to blockages in fluid pathways as a result of damage to the network. Despite recent advances in printing soft, biomimetic materials [31], the creation of multi-dimensional, interconnected and redundant microvascular networks like those found in natural materials [32] has remained an unmet challenge in fiber-composites.

This paper describes, for the first time, the fabrication of 3D interconnected (Fig. 1e) microvascular networks within a fiber-reinforced polymer composite. These vascular architectures are realized through advancements in catalyst dispersion, melt-spinning of sacrificial fibers with post-processing to improve their mechanical properties, and melt-extrusion of sacrifical filament for 3-D printing. Tuning the sacrificial PLA degradation kinetics and fiber mechanical properties enables seamless composite textile preform integration, survival during FRC processing, and consistent *in situ* evacuation within cured composites. Two types of complex microvascular architectures are constructed in FRC prototypes to demonstrate the versatility and scope of advanced VaSC processing methods.

2. Materials and methods

2.1. Sacrificial material preparation

Sacrificial poly(lactic acid) (PLA) was prepared by combining commercial PLA with varying concentrations of tin (II) oxalate (SnOx) catalyst. Both solution and melt-blending [33] techniques were explored to produce a uniform dispersion of catalyst within PLA for improved evacuation (VaSC) characteristics.

2.1.1. SnOx catalyst particle sizing

Since the sacrificial PLA/SnOx material is used to create vascular precursors with features on the micro-scale (typically between 100–500 μm), the as received SnOx (Sigma-Aldrich) particulates are either sieved (U.S. Std. No. 500) or further ground in a high-speed rotary mixer (Col-Int Tech, FW-100) in 100 g batches for several minutes to ensure particle sizes less than 25 μm. Catalyst powder was stored in an atmospheric desiccator to prevent clumping.

2.1.2. Solvent blending SnOx and PLA

Solvent blending was performed by combining 20 g of PLA (4043D [34], Natureworks LLC, $M_w \approx 150$ kDa [35]) in a glass container with 200 mL of dichloromethane (DCM) and sealed until the PLA was fully dissolved; typically 24 h with intermittent manual agitation. The desired proportion of SnOx (per wt% of PLA) was then added to the solution and shaken until uniformly dispersed. Immediately after agitation (before particle settlement), the

viscous mixture was poured into a rectangular glass pan (250 × 350 mm areal dimensions) and dried for 24–48 h in a fume hood.

2.1.3. Melt compounding SnOx and PLA

Melt blending/compouding was performed with a twin-blade measuring mixer (Type Six, Brabender®) heated to 170 °C after which 60 g of PLA (4043D, Natureworks LLC) was added to the chamber while rotating the mixing blades at 15 RPM until completely melted. The desired proportion of SnOx (per wt% of PLA) was slowly added and then mixed at 45 RPM for 15 min. The melt-compounded SnOx/PLA was extracted from the chamber and cut while still pliable, into irregular pieces with nominal dimensions less than 25 × 15 × 15 mm. Melt-compounding and pelletizing (3 × 3 × 4 mm) on the kilogram batch scale was achieved through an industrial development partner (Polymers Center of Excellence, Charlotte, NC).

2.2. Sacrificial template fabrication

The blended sacrificial polymer was first dried in an oven at 70 °C under vacuum (13 Torr) for at least 6 h to remove any additional solvent or moisture that could lead to hydrolitic degradation of PLA [33,36,37]. The dried material was then used as feedstock for sacrificial template fabrication by fiber-spinning, filament extrusion, and fused deposition modeling.

2.2.1. Fiber spinning

Sacrificial fibers (550–850 μm diameter) were produced using a modified lab-scale melt-spinning apparatus. Sacrificial polymer (≈30 g) was loaded into a steel barrel and allowed to melt for 45 min at 175 °C. Next, a polytetrafluoroethylene (PTFE) disk followed by brass capped steel piston were inserted into the top barrel opening and mechanically advanced to extrude SnOx/PLA material through a 1.25 mm diameter spinneret at a rate of approximately 5.5 g/min. The extruded fiber was guided over a metal pulley and laterally translated to provide uniform spooling around the winding reel. The rotational speed of the take-up reel (88 mm diameter) was adjusted to control fiber size. At a winding rate of 33 RPM, a single extrusion run produced roughly 50 m of 750 ± 20 μm diameter fiber.

2.2.2. Filament extrusion

Filament feedstock (≈3 mm diameter) for fused deposition modeling (FDM) was initially produced using the same melt-spinning apparatus (at 175 °C) by extruding sacrificial polymer through a brass spinneret extension (75 mm long, 2.5 mm ID) into a room temperature (RT) water column roughly 1.2 m tall. Resulting filaments ranged from 2.4 mm to 3.1 mm in diameter, within printable tolerances for the FDM equipment. Higher volume production of FDM filament with improved dimensional stability was carried out through a proprietary industrial collaboration (CU AerospaceLLC).

2.2.3. Fused deposition modeling (FDM)

3-D printing via FDM was performed with an extrusion nozzle diameter of 0.35 mm, a nozzle temperature of 175 °C, and a heated print bed at 60 °C. The printer bed was covered with polyethylene terephthalate (PET) tape and roughened with light sanding to enhance surface adhesion of the printed material. The total print time for a sacrificial template, including the calibration border, was approximately 1 min. The bed temperature was lowered to 40 °C before removing the network templates and a final trimming.

2.3. SnOx particle visualization

Visualization of SnOx catalyst particles within PLA polymer was carried out by X-ray computed microtomographic (μCT) imaging on an Xradia MicroXCT-400. Scans covering 182° were obtained in rotation intervals of 0.25° using a 20x objective (1 μm per pixel resolution) at 5 s exposure times with 40 kV (200 μA, 8 W) source settings. 3D reconstructions were performed in Xradia TXM Reconstructor software (v. 8.1.7546) and cross-sectional image slices reproduced via Xradia TXM Controller (v. 8.1.7546).

2.4. Isothermal thermogravimetric analysis (iTGA)

iTGA experiments were performed on a Mettler-Toledo TGA851^e, calibrated with indium, aluminum, and zinc standards. For each experiment, the sample (ca. 8 mg) was accurately weighed (±0.02 mg) in an alumina crucible. The mass loss was recorded while heating from 25 °C to the desired temperature at 20 °C/min, and then holding temperature constant for 16 h, entirely under continuous nitrogen gas purge.

2.5. Gel permeation chromatography (GPC)

Analytical GPC analyses were performed on a system composed of a Waters 1515 Isocratic high pressure liquid chromatography pump, a Waters (2414) Refractive Index (RI) Detector, a Waters (2707) 96-well autosampler, and a series of 4 Waters HR Styragel columns (7.8 × 300 mm, HR1, HR3, HR4, and HR5) in tetrahydrofuran (THF) at 30 °C. The GPC was calibrated using monodisperse polystyrene (PS) standards. Various types of PLA/SnOx samples (ca. 15 mg) were placed in scintillation vials (4 mL) and freeze-dried prior to GPC measurements in order to remove any water. Subsequently, 2 mL of dry THF was injected into the vials using a syringe and magnetic stir-bars were used to facilitate dissolution. After securing the lid, vials were placed on a stir plate (150–200 RPM) for 4 h at room temperature (RT). A vial containing neat PLA was heated at 50 °C to promote dissolution of crystalline domains. No precipitation occurred after cooling to RT for any samples. Polymer solutions were injected via a 1 mL syringe into 300 μL GPC vials through a 0.45 μm polytetrafluoroethylene (PTFE) filter to remove SnOx catalyst particles. Vials were inserted in the GPC autosampler tray and each sample type was run in continuation with two consecutive injections (each 60 min) according to standard instrument protocol. Number and weight averaged molecular weights (M_n and M_w) were calculated using Wyatt's Astra 6 software through integration of the signal peaks obtained from the RI detector using the latest PS calibration.

2.6. Differential Scanning Calorimetry (DSC)

Differential scanning calorimetry (DSC) was performed on a TA Instruments Q20 module calibrated with indium and zinc standards. Dynamic experiments were conducted in hermetically sealed Tzero™ aluminum crucibles under a nitrogen atmosphere to measure heat flow (positive exotherm) during a temperature sweep from 0 to 300 °C at a heating rate of 10 °C/min.

2.7. Single-fiber tension tests

Single PLA fibers were loaded in direct tension according to ASTM D3822 [38] provisions using a TA Instruments' RSA3 mechanical analyzer. The fiber gauge length was 25 mm and adhesively-bonded paper loading tabs were used to align and grip the sample in the test fixture. Quasi-static testing was performed in displacement-control mode at a rate of 300 μm/min until

complete failure (i.e. fracture) or an engineering strain (ϵ) of approximately 18% was reached.

2.8. FRC processing

2.8.1. Automated 3-D weaving

A hybrid glass/carbon/sacrificial PLA fiber preform was woven at the North Carolina State University College of Textiles using an automated 3-D weaving machine [39] in a 3WEAVE™ [40] non-crimp orthogonal pattern. The 3D fiber preform consisted of 2 warp layers of continuous filament E-glass yarn (EC6-136 1X0 Z40 636, AGY Corp.) and 3 weft/fill layers, where the central fill layer was a double insertion of the E-glass yarn, and the top and bottom fill layers consisted of 3 k carbon-fiber tows (Granoc YSH-65A, Nippon Graphite Fiber Corp.) at 14 picks per inch. Sacrificial PLA z-fibers (36 total, 300 μm diameter) were interwoven along the warp direction with a spacing of approximately 280 μm between adjacent fibers (see Fig. 6).

2.8.2. Fiber preform layups

The layup sequence for a 3D composite laminate from bottom to top consisted of: **(1)** five layers (25 × 115 mm) of 2D plain weave E-glass fabric (CST G10800 47.5 g/m^2); **(2)** a hybrid (carbon/glass) 3D woven preform with sacrificial PLA z-fibers (25 × 115 mm); **(3)** and five layers identical to **(1)** above.

The layup sequence for a 2D composite laminate containing sacrificial, network precursors from bottom to top consisted of: **(i)** four layers (250 × 230 mm) of $[90/0]_2$ 8H satin weave E-glass (0.31 kg/m^2) (Style 7781, Fibre Glast Developments Corp.); **(ii)** eight layers (250 × 230 mm) of $[90/0]_4$ 8H satin weave E-glass with through-stitched sacrificial fibers restraining 3D printed, branched network templates on the top surface (see Fig. 9); and **(iii)** another four layers identical to **(i)** above.

2.8.3. Vacuum assisted resin transfer molding (VARTM)

Prior to fiber preform infusion, epoxy resin (Araldite LY 8605) and amine hardener (Aradur 8605) components (Huntsman Advanced Materials LLC) were combined (80 g resin: 28 g hardener, 35 pph by weight), mixed, and degassed at RT under 12 Torr vacuum (abs) for a total of 3 h (Yamato ADP31 drying oven, Welch 1402 vacuum pump).

VARTM was performed by applying 38 Torr (abs) vacuum (Welch DryFast® Tuneable Chemical-Duty Vacuum Pump: model 2032B) until complete fabric wetting and then decreasing vacuum to 76 Torr (abs) for 36 h at room temperature (RT) until resin solidification. The composite panel was then cured for 2 h at 121 °C followed by 3 h at 177 °C in a convection oven (Thermo Scientific Lindberg/Blue M). The glass transition temperature (T_g = 152 °C) of the epoxy matrix was measured after cure according to ASTM E1356 [41] and is reported as the inflection (midpoint) of the endotherm.

2.8.4. Vaporization of sacrificial components (VaSC)

Composite samples were cut using a diamond-blade wet saw to expose sacrificial fiber cross sections and then wet-sanded (240 grit) until smooth. Air-dried samples were then placed in an evacuation oven (Jeio Tech Co., Ltd. OV-11) at room temperature (RT) and heated to 200 °C for 16 h under 12 Torr (abs) vacuum. After cooling to RT the evacuated, microvascular composite was removed. The vasculature was then flushed with water to verify evacuation followed by compressed air for final clearing.

2.8.5. Microvascular network visualization

Visualization of vasculature within the FRCs was performed by X-ray computed microtomographic (μCT) imaging on an Xradia MicroXCT-400. μCT scans were conducted after filling the empty microchannels with iohexol (Omnipaque™ 350) serving as a radiocontrast agent.

For the 3D hybrid composite laminate, 198° scans were obtained in rotation intervals of 0.25° using a 1.0x objective

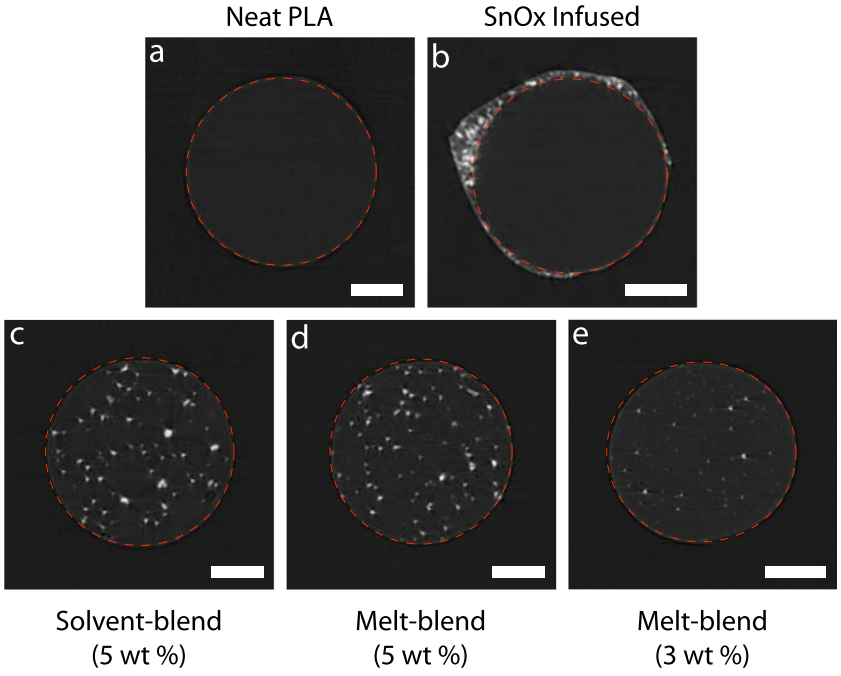

Fig. 2. X-ray computed microtomography (μCT) cross-sectional images of various PLA fiber types revealing distribution of SnOx catalyst particles (white). (a) Neat PLA (4043D, Natureworks LLC) fiber; (b) Catalyst-infused [24] commercial PLA monfilament (Nextrusion GmbH) showing surface agglomeration of SnOx; (c) Solvent-blended, melt-spun fiber with 5 wt%, sieved SnOx catalyst; (d) Melt-blended, melt-spun fiber with 5 wt%, sieved SnOx catalyst; (e) Melt-blended, melt-spun fiber with 3 wt%, ground SnOx catalyst particles (<25 μm) (scale bars = 100 μm).

(20 μm per pixel resolution) at 10 s exposure times with 60 kV (133 μA, 8 W) source settings.

For the 2D composite laminate, 204° scans were obtained in rotation intervals of 0.25° using a 0.5x objective (40 μm per pixel resolution) at 1 s exposure times with 60 kV (133 μA, 8 W) source settings.

Scan reconstructions were performed using Xradia TXM Reconstructor software (v. 8.1.7546). Images were produced via Xradia TXM 3D Viewer and Amira™ (v. 5.5.0).

2.9. Microscopy

Compiled optical images were acquired on a Keyence VHX-5000 digital microscope at 150x magnification using automated stitching. Scanning electron micrographs (SEM) were acquired on a Phillips XL30 ESEM-FEG at 2 kV, after sputter-coating the samples with gold/palladium for 60 s using a Denton Desk II TSC-turbo pumped unit. National Institute of Health's (NIH) Image J software was used for digital measurements.

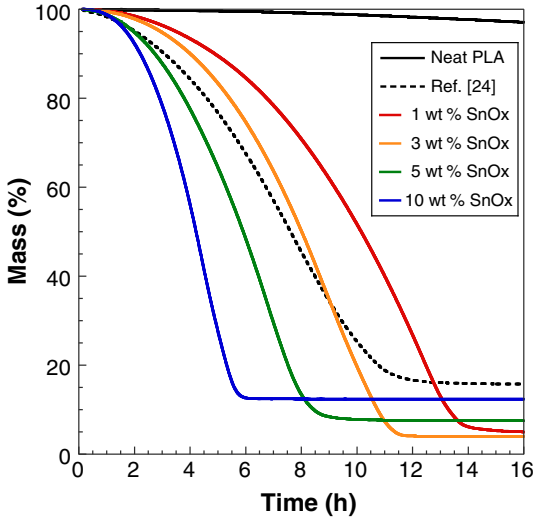

Fig. 3. Isothermal thermogravimetric analysis (iTGA) of various solvent-blended SnOx/PLA (sieved catalyst) combinations at 200 °C for 16 h. (Dashed line represents sacrificial fibers prepared via solvent-swelling according to provisions in Ref. [24]). (For interpretation of the references to color in this figure legend, the reader is referred to the web version of this article.)

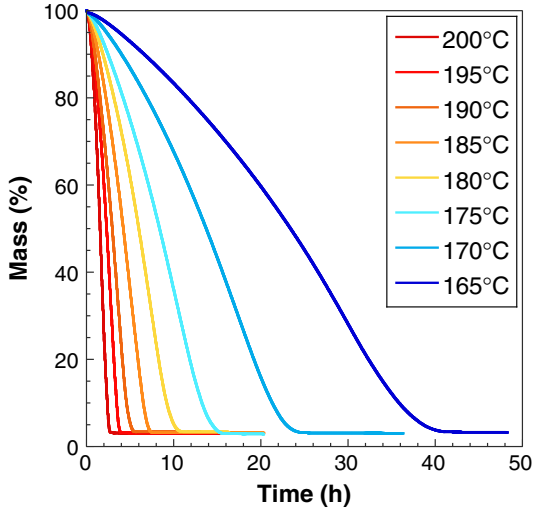

Fig. 4. Isothermal thermogravimetric analysis (iTGA) of melt-compounded sacrificial PLA/SnOx (3 wt% ground SnOx) at various temperatures. (For interpretation of the references to color in this figure legend, the reader is referred to the web version of this article.)

3. Characterization of sacrificial polymer

3.1. Catalyst distribution

The distribution of SnOx catalyst particles within PLA fibers after various processing conditions was investigated by μCT. Fibers produced from both solvent- and melt-blended polymer feedstock exhibited uniform SnOx catalyst distribution in contrast to surface agglomeration apparent in catalyst-infused [24] commercial fibers (Fig. 2). Imaging of melt-blended sacrificial fibers containing ground SnOx catalyst confirmed that smaller sized particles are achieved when compared to as-received, and sieved catalyst (Figs. 2d vs. 2e).

3.2. Mass loss

The depolymerization and vaporization of solvent-blended PLA was assessed by isothermal thermogravimetric analysis (iTGA) at 200 °C for 16 h, and compared to neat PLA and prior catalyst-infused sacrificial fibers [24]. Representative iTGA traces (Fig. 3)

Table 1
Molecular weights of sacrificial PLA/SnOx determined by gel permeation chromatography (GPC) after various stages of thermal processing.

Material type	M_n (kDa)	M_w (kDa)
Neat PLA pellets (4043D)	143.7 ± 0.70[a]	237.1 ± 0.23
PLA/SnOx[b] pellets	105.3 ± 0.88	156.3 ± 0.19
Sacrificial filament (≈3 mm)	91.0 ± 0.50	155.5 ± 0.26
Commercial-spun fiber (≈300 μm)	89.6 ± 2.52	145.8 ± 2.10
Commercial-spun fiber (≈900 μm)	95.4 ± 0.14	152.0 ± 0.34
Lab-spun fiber (≈300 μm)	87.3 ± 1.93	140.5 ± 0.02
3-D printed template	74.8 ± 1.00	123.4 ± 0.52

[a] Error represents standard deviation from two GPC measurements.
[b] 3 wt% SnOx.

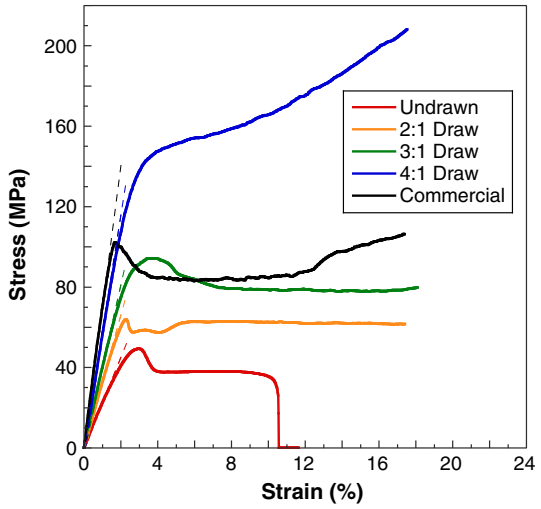

Fig. 5. Representative tensile stress versus strain behavior for various PLA fiber samples. Neat commercial fiber (Nextrusion GmbH) is tested as received for reference. All other fibers were melt-compounded and melt-spun containing 3 wt% SnOx where an increased draw ratio resulted in stiffer and stronger fibers. [Note: Dashed lines represent elastic modulus (E) calculated up to 1% strain]. (For interpretation of the references to color in this figure legend, the reader is referred to the web version of this article.)

Table 2
Summary of average mechanical properties from single-fiber tensile tests.

Fiber type	Diameter (μm)	Yield stress (MPa)	Yield strain (%)	Modulus[a] (GPa)
Undrawn	740 ± 40[b]	48.7 ± 1.6	2.9 ± 0.1	2.1 ± 0.2
2:1 Draw	455 ± 25	61.5 ± 4.7	2.5 ± 0.4	3.2 ± 0.3
3:1 Draw	385 ± 15	89.4 ± 4.7	2.8 ± 0.1	4.1 ± 0.1
4:1 Draw	320 ± 5	135.0 ± 2.3	3.0 ± 0.0	5.7 ± 0.1
Commercial	200 ± 1	102.1 ± 1.8	1.8 ± 0.1	6.8 ± 0.2

[a] Elastic modulus calculated up to 1% strain.
[b] Error represents standard deviation from three samples.

show that neat PLA exhibits less than 5% weight loss over the entire 16 h time interval, whereas both solvent-blended and catalyst-infused sacrificial fibers demonstrate complete depolymerization and vaporization during the course of the experiment with a residual mass roughly equivalent to the initial concentration of SnOx used. As SnOx catalyst concentration increases (1, 3, 5, 10 wt%) the time to achieve complete PLA evacuation decreases (≈15, 12, 9, 6 h), respectively. Thus, a trade-off exists between PLA evacuation time and residual mass (catalyst). Catalyst-infused fibers [24] show the largest residual mass (SnOx), and was revealed by μCT to be surface agglomerations of catalyst particles (Fig. 2b).

A catalyst concentration of 3 wt% was ultimately selected for use with commercial melt-compounding and pelletizing as it provided a balance between evacuation time and residual mass in the solvent-blended studies. The commercially melt-compounded PLA/SnOx exhibited the fastest overall evacuation time (≈3 h) at 200 °C (Fig. 4) as a result of increased catalyst surface area from the use of smaller size (ground) catalyst particles. Depolymerization of this melt-blended material was also explored at a series

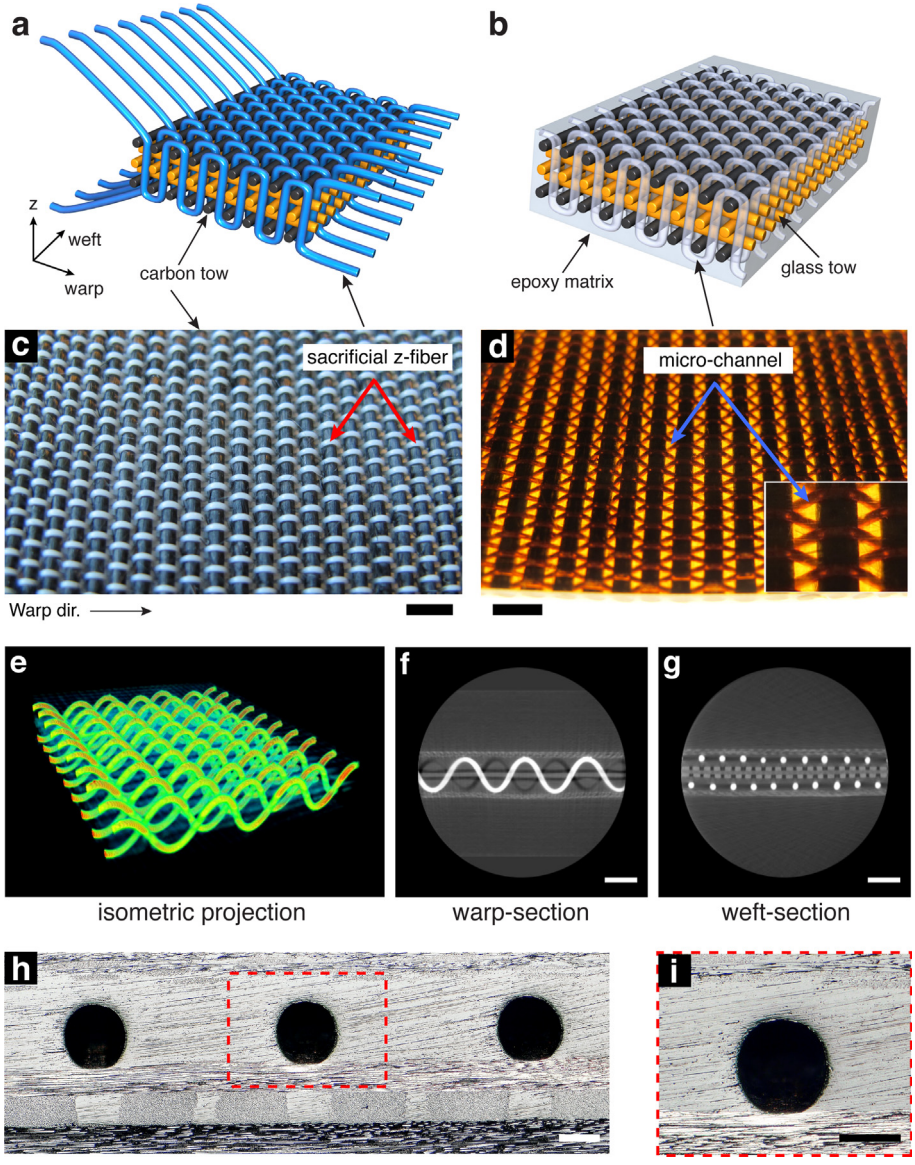

Fig. 6. 3-D woven, hybrid microvascular composite. (a) Schematic of 3WEAVE™ non-crimp orthogonal, carbon/glass reinforcement co-woven with sacrificial PLA z-fibers; (b) Schematic of vascular composite after resin infiltration/solidification and subsequent vaporization of sacrificial components (VaSC); (c) Optical image of textile preform with 300 μm diameter sacrificial z-fibers; (d) Optical image of fiber-reinforced composite (post-VaSC) revealing closely spaced rows (≈280 μm) of microchannels; (e) Isometric reconstruction from μCT scan of sinusoidally undulating microchannels filled with liquid radiocontrast agent; (f) 2D μCT slice (warp-dir.) along microchannel centerline revealing sandwiched 3D woven composite between confining glass-fiber layers; (g) 2D μCT slice (weft-dir.) across microchannel crest/trough line, revealing spacing fidelity between adjacent microchannels; (h, i) optical images showing circularity of microchannel cross-sections (scale bars: c-d = 3 mm, f-g = 2 mm, h-i = 250 μm). (For interpretation of the references to color in this figure legend, the reader is referred to the web version of this article.)

of temperatures below 200 °C. While the amount of time to achieve complete depolymerization increases as temperature is decreased, the ability to evacuate the sacrificial polymer at temperatures below 200 °C provides added flexibility in terms of processing conditions and host material selection.

3.3. Molecular weight

Gel permeation chromatography (GPC) was conducted on sacrificial materials (Table 1) to measure molecular weight degradation after various thermal processing steps. 3-D printed templates exhibited the greatest reduction (≈50%) in molecular weight as compared to neat PLA pellets ($M_n \approx 145$ kDa). GPC results reveal a 25% reduction in molecular weight occurs during the initial melt-compounding and pelletizing process. Further processing into filament and printing accounts for the remaining 25% reduction in molecular weight. All sacrificial PLA/SnOx materials produced were robust enough to survive subsequent FRC manufacturing under normal handling, compaction, and infusion conditions.

3.4. Mechanical performance

Melt-spun fibers were mechanically fragile after the spinning process. Post-processing of the fibers by drawing (stretching) at 80 °C, which is above the glass transition temperature ($T_g \approx 57$ °C) [35] and below the melting temperature ($T_m \approx 160$ °C) [34] of PLA, improved mechanical properties due to increased orientation (crystallinity) of polymer chains [33,36,37].

To produce sacrificial fibers suitable for use in FRC manufacturing, an automated drawing machine was designed and constructed to achieve draw ratios ranging between 2:1–4:1 (final:original length). Post-drawn fibers exhibited less variation in diameter with increasing draw ratio compared to melt-spun fibers taken directly off the winding reel. Drawn fibers were tested in uniaxial tension and representative stress-strain (σ-ϵ) behavior is presented in Fig. 5. As the draw ratio increases, both the elastic modulus (E) and yield stress (σ_y) increase substantially. In comparison to an undrawn fiber, drawn fibers at 2:1, 3:1, and 4:1 ratios exhibited a 1.3, 1.8, and 2.8-fold increase in yield stress and 1.5, 2.0, and 2.7-fold increase in elastic modulus, respectively. Enhanced post-yield ductility and strain hardening is also evident as the draw

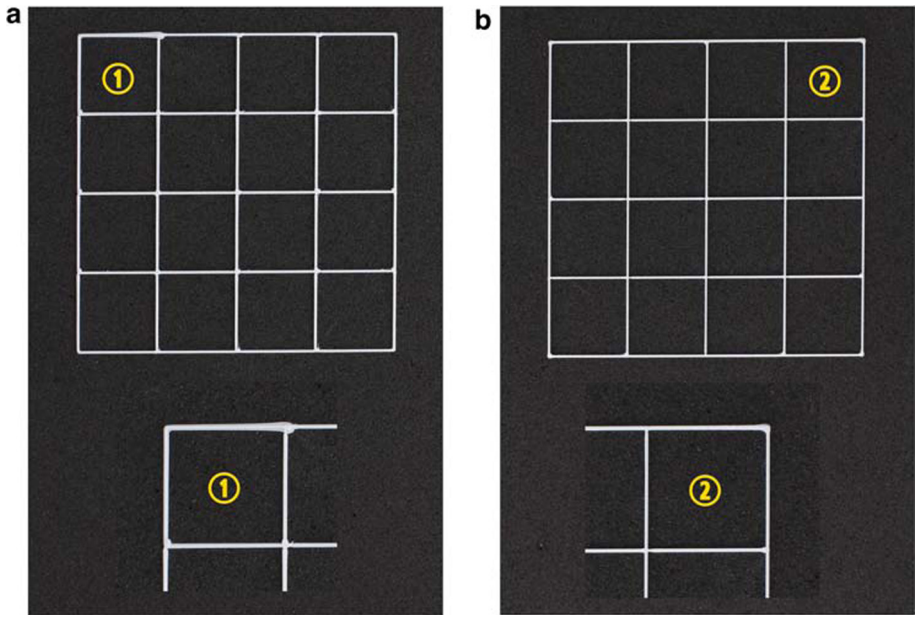

Fig. 7. 3-D printed calibration grids. Printed sacrificial templates from the (a) auto-generated and (b) manually edited G-code input files with zoomed inset (grid unit cells are 15 × 15 mm).

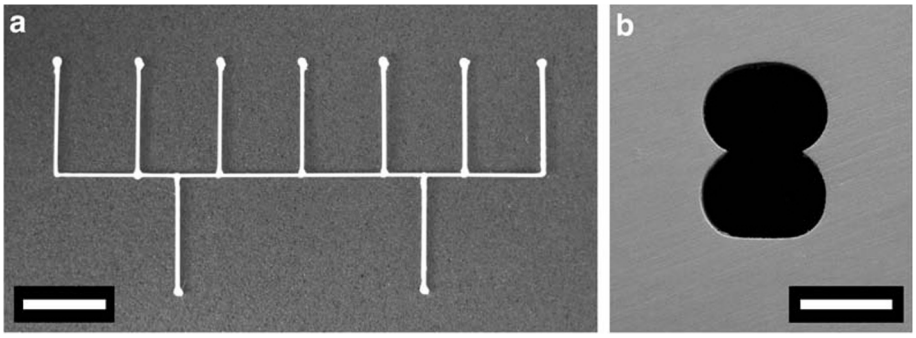

Fig. 8. 3-D printed vascular template. (a) Optical image of microvascular network precursor with orthogonal branching; (b) Scanning electron micrograph (SEM) of evacuated channel cross-section with "hourglass" geometry resulting from dual-layer FDM construction (scale bars: a = 10 mm, b = 300 μm).

ratio increases, which enables weaving of sacrificial fibers into structural fiber preforms at potentially small radii of curvature. A summary of the average yield stress, yield strain (ϵ_y) and elastic modulus for all fibers is provided in Table 2.

4. Results

4.1. 3-D woven vascular composite

The construction of a prototype microvascular composite heat exchanger containing tightly woven and densely packed sacrificial fibers was undertaken to demonstrate the capability of melt-spun and drawn PLA/SnOx fiber in FRC manufacturing. The vascular composite is intended for use as a counterflow Joule-Thomson cooler for infrared cameras, superconducting electronics, gamma ray detectors, and other devices requiring cryogenic temperatures. Microvascular heat exchangers that are low cost, compact, and highly efficient will enable a new class of Joule-Thomson cryocoolers [42]. The device architecture consists of a 3D, non-crimp orthogonal [40] "hybrid" reinforcement textile (Fig. 6) including glass, carbon, and sacrificial PLA fibers (300 μm) that were co-woven on a 3D micro-weaving machine [39]. As a direct result of superior mechanical properties of melt-spun and drawn sacrificial fibers, no fiber breakage occurred during automated weaving and high-regularity in computer-controlled placement was achieved.

The resulting 3D microvascular composite (Fig. 6d) consists of a parallel arrangement of closely spaced (≈280 μm gap), sinusoidally undulating microchannels along the warp direction (5.8 vol%). The empty vasculature was filled with a liquid, radiocontrast agent and imaged using μCT to visualize vascular architecture and verify evacuation fidelity (Fig. 6e-g). High resolution optical imaging of the cross-section reveals that the channels largely retain their circular profile although some flattening occurs during compaction at the bottom crown of the channel next to the adjacent carbon fiber tow (Fig. 6h,i). The relatively high volume fraction of microchannels coupled with their close packing will likely affect some mechanical properties [13,14,30,43–45]. Ultimately, the design of vascular heat exchangers must balance both thermal and mechanical performance metrics simultaneously.

4.2. 3-D printed architectures

Interconnected, sacrificial templates were printed using a desktop FDM (AO-100, Lulzbot). Two routes for creating the G-code input files that dictate print pathways were evaluated. In the first approach, a solid model of the geometry was created via CAD (SolidWorks v.2011, Dassault Systèmes) and converted to stereolithography (STL) data format. The STL file was then converted to instructional G-code using open source software (Slic3r v.0.9.10b). In the second approach, G-code files were manually written and edited through an iterative process starting from extrusion and movement parameters defined in the auto-generated files. A uniform grid (4 × 4) structure printed using both approaches was compared to assess differences in printing precision (Fig. 7). Direct observation of the printing process as well as measurement of the final sacrificial templates both support the conclusion that manual generation of G-code files is necessary to achieve high-fidelity lattice printing on the micron-scale. Print consistency is especially important for microvascular architectures since small variations in cross-section are magnified by pressure fluctuations that scale by the fourth power of hydraulic diameter for laminar flow according to the Hagen-Poiseuille relation [46].

Optical imaging of a branched network template (Fig. 8a) and subsequent scanning electron microscopy of an evacuated cross-section (Fig. 8b) revealed an "hourglass" shape that is the result of printing two consecutive layers. For the specified printing conditions, each lobe was roughly equivalent in cross-sectional area (0.099 mm^2) to that of a 360 μm diameter, circular channel (0.10 mm^2).

4.3. 3D interconnected composite vasculature

Redundant vascular interconnections (Fig. 1) are important for sustained fluid delivery in the presence of damage. Inspired by biological vascular redundancy, such as the leaf venation of *Citrus limon* [32], a 3D interconnected microvascular network was constructed in an FRC by joining melt-spun sacrificial fibers with printed sacrificial templates.

A 2D woven, glass-fiber composite preform (8H satin, $[90/0]_4$) was prepared by hand stitching melt-spun and drawn sacrificial PLA fibers (300 μm) in a parallel undulating configuration, so that the fibers restrain two branched PLA/SnOx network templates onto the glass fabric (Fig. 9a). The through-thickness sacrificial fibers and branched network templates were then solvent-welded at the points of contact using a solution of PLA/SnOx in DCM (PLA/SnOx/DCM: 1/20/100 by wt). After air drying at RT for least 48 h, 4 layers of 8H satin fabric were placed on both the top and bottom of the stitched preform. A FRC laminate (Fig. 9b) was then fabricated by infusing the preform with epoxy resin using VARTM and curing.

After a post-cure thermal treatment of 200 °C for 16 h, the evacuation (VaSC) of the conjoined sacrificial elements produced a 3D interconnected, microvascular network within the composite laminate. The network of microchannels was visualized by filling the

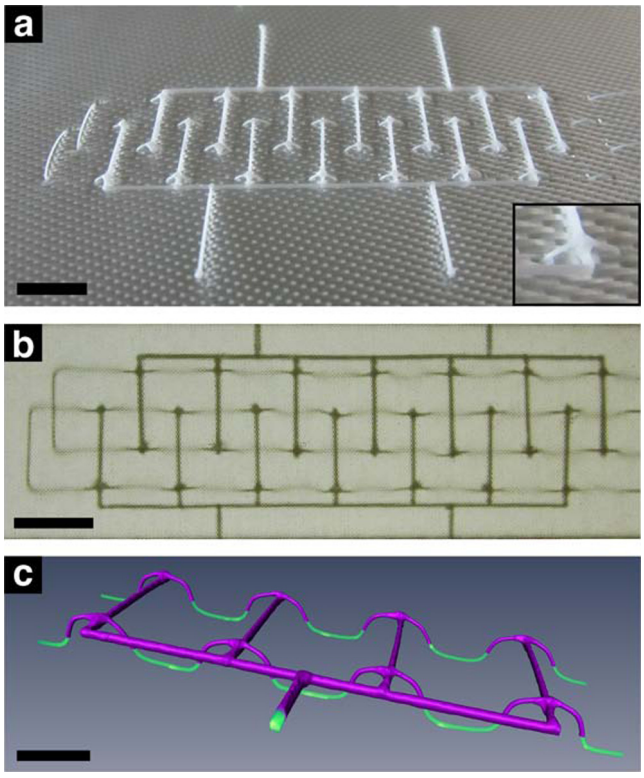

Fig. 9. Hierarchical, microvascular fiber-composite fabrication. (a) Layered, 2D woven (*E*-glass) reinforcement with stitched (through-thickness) sacrificial PLA fibers that are solvent-welded to planar branched network templates; (b) Optical image of fiber-reinforced composite containing network template prior to VaSC; (c) μCT reconstruction showing portion of 3D, interconnected microvasculature after VaSC (scale bars: a,b = 10 mm, c = 5 mm). (For interpretation of the references to color in this figure legend, the reader is referred to the web version of this article.)

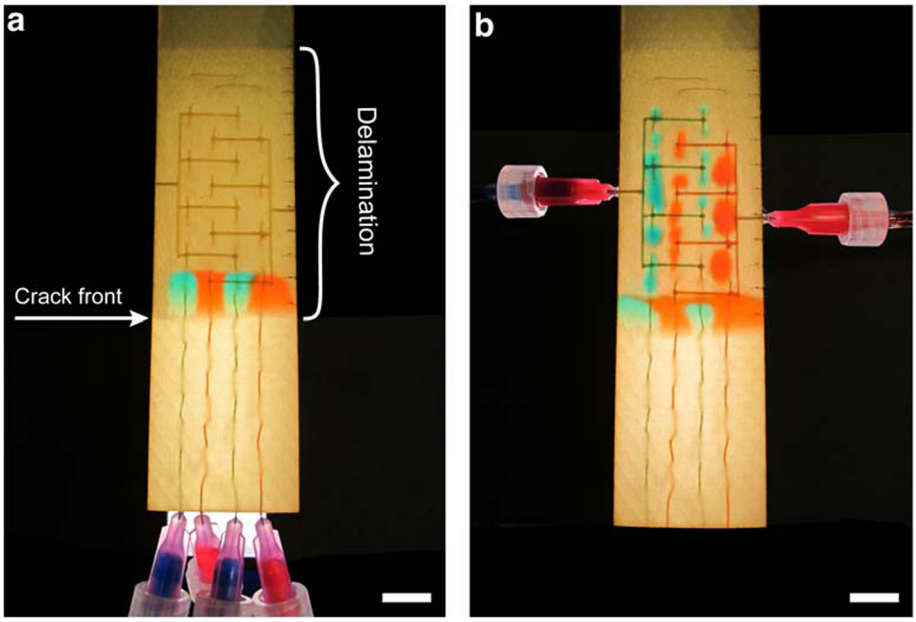

Fig. 10. Redundant vascular networks circumvent damage in fractured composite. (a) Delivery of liquid agents (red/blue) to a mid-plane delamination through parallel (segregated) micro-channels isolates flow to the crack front alone; (b) Delivery via branched (redundant) networks circumvents damage and provides fluid access to the entire fracture plane (scale bars = 10 mm). (For interpretation of the references to color in this figure legend, the reader is referred to the web version of this article.)

empty vasculature with a liquid, radiocontrast agent and imaging by μCT (Fig. 9c).

To demonstrate redundant flow capabilities enabled by synthetic, interconnected vasculature, dyed liquids were delivered via different network pathways to vascular orifices created by a mid-plane delamination in the glass-fiber composite. Delivery through the parallel (segregated) microchannels (Fig. 10a) limits fluid access to only four vascular openings at the crack (delamination) front. A large portion of the fracture surface remains dry and is inaccessible to liquid delivery. Yet, efficient self-healing requires access to the entire delalmination [30], a condition that can only be achieved by external intervention (liquid pumping or mechanical cycling of the crack opening). In stark contrast, delivery through the branched portions of the microvascular network (Fig. 10b) provides efficient liquid dispersion across the entire fracture surface. In this case, the severed parallel microchannels are circumvented by delivery through the redundant, branched (planar) networks residing in a layer above the delamination. The 3D interconnected nature of the vascular network makes comparison to prior studies of the mechanical integrity of vascular composites exceedingly difficult [13,14,30,43–45]. Although it has been shown in one study that through thickness microchannels alone can increase delamination resistance via crack tip blunting [30], the full impact of complex, 3D networks on mechanical properties remains to be investigated.

5. Conclusions

A variety of thermal processing techniques for sacrificial microvascular templates have been developed by uniform dispersion of small (<25 μm) SnOx catalyst particles within PLA [47]. Sacrificial fibers tailored for strength and ductility were produced by melt-spinning at 175 °C followed by drawing at 80 °C over a range of draw ratios. 3D printed sacrificial templates were produced by FDM of 3 mm diameter filament feedstock. The melt-spun fibers and printed templates are mechanically robust and they survive and maintain their form factor during conventional FRC manufacturing. By combining both types of sacrificial elements, 3D interconnected microvasculature was created in a FRC that exhibits damage redundant flow inspired by biological systems. These types of vascular architectures may find utility not only for self-healing, but also for a variety of multifunctional applications including thermal management and electromagnetic reconfigurability.

Acknowledgments

This work was supported by the Air Force Office of Scientific Research (award numbers FA9550-16-1-0017 and FA9550-14-C-0010). J.F. Patrick is grateful to the Arnold and Mabel Beckman Foundation for financial support through the Beckman Institute Postdoctoral Fellowship at the University of Illinois Urbana-Champaign (UIUC). The authors acknowledge Dr. Alex Bogdanovich in the Department of Textile Engineering at North Carolina State University for 3-D weaving, Dr. Jeffrey Olson at Lockheed Martin Space Systems Company for insightful heat-exchanger discussion, and Darren King at CU Aerospace LLC for construction of the fiber-drawing machine. In addition, the authors thank undergraduate research assistants Laura Richardson and Yelizaveta Fedonina for assistance with preform stitching and 3-D printing, respectively.

References

[1] Therriault D, White SR, Lewis JA. Chaotic mixing in three-dimensional microvascular networks fabricated by direct-write assembly. Nat Mater 2003;2:265–71.
[2] Therriault D, Shepherd RF, White SR, Lewis JA. Fugitive inks for direct-write assembly of three-dimensional microvascular networks. Adv Mater 2005;17:395–9.
[3] Toohey KS, Sottos NR, Lewis JA, Moore JS, White SR. Self-healing materials with microvascular networks. Nat Mater 2007;6:581–5.
[4] Toohey KS, Hansen CJ, Lewis JA, White SR, Sottos NR. Delivery of two-part self-healing chemistry via microvascular networks. Adv Funct Mater 2009;19:1399–405.
[5] Hansen CJ, Wu W, Toohey KS, Sottos NR, White SR, Lewis JA. Self-healing materials with interpenetrating microvascular networks. Adv Mater 2009;21:4143–7.
[6] Hamilton AR, Sottos NR, White SR. Self-healing of internal damage in synthetic vascular materials. Adv Mater 2010;22:5159–63.

[7] Hansen CJ, White SR, Sottos NR, Lewis JA. Accelerated self-healing via ternary interpenetrating microvascular networks. Adv Mater 2011;21:4320–6.
[8] Bleay SM, Loader CB, Hawyes VJ, Humberstone L, Curtis PT. A smart repair system for polymer matrix composites. Compos Part A: Appl Sci Manuf 2001;32:1767–76.
[9] Pang JWC, Bond IP. A hollow fibre reinforced polymer composite encompassing self-healing and enhanced damage visibility. Compos Sci Technol 2005;65:1791–9.
[10] Trask RS, Bond IP. Biomimetic self-healing of advanced composite structures using hollow glass fibres. Smart Mater Struct 2006;15:704–10.
[11] Trask RS, Williams GJ, Bond IP. Bioinspired self-healing of advanced composite structures using hollow glass fibres. J Roy Soc Interface 2007;4:363–71.
[12] Williams GJ, Trask RS, Bond IP. A self-healing carbon fibre reinforced polymer for aerospace applications. Compos Part A: Appl Sci Manuf 2007;38:1525–32.
[13] Kousourakis A, Mouritz AP, Bannister MK. Interlaminar properties of polymer laminates containing internal sensor cavities. Compos Struct 2006;75:610–8.
[14] Kousourakis A, Mouritz AP, Bannister MK. Tensile and compressive properties of polymer laminates containing internal sensor cavities. Compos Part A: Appl Sci Manuf 2008;39:1394–403.
[15] Huang CY, Trask RS, Bond IP. Characterization and analysis of carbon fibre reinforced polymer composite laminates with embedded circular vasculature. J Roy Soc Interface 2010;7:1229–41.
[16] Norris CJ, Bond IP, Trask RS. Interactions between propagating cracks and bioinspired self-healing vascules embedded in glass fibre reinforced composites. Compos Sci Technol 2011;71:847–53.
[17] Norris CJ, White JAP, McCombe G, Chatterjee P, Bond IP, Trask RS. Autonomous stimulus triggered self-healing in smart structural composites. Smart Mater Struct 2012;21:1–10.
[18] Norris CJ, Bond IP, Trask RS. Healing of low-velocity impact damage in vascularised composites. Compos Part A: Appl Sci Manuf 2013;44:78–85.
[19] Coope TS, Wass DF, Trask RS, Bond IP. Repeated self-healing of microvascular carbon fibre reinforced polymer composites. Smart Mater Struct 2014;23:1–16.
[20] Trask RS, Norris CJ, Bond IP. Stimuli-triggered self-healing functionality in advanced fibre-reinforced composites. J Intell Mater Syst Struct 2014;25:87–97.
[21] Trask RS, Bond IP. Bioinspired engineering study of plantae vascules for self-healing composite structures. J Roy Soc Interface 2010;7:921–31.
[22] Norris CJ, Bond IP, Trask RS. The role of embedded bioinspired vasculature on damage formation in self-healing carbon fibre reinforced composites. Compos Part A: Appl Sci Manuf 2011;42:639–48.
[23] Norris CJ, Meadway GJ, O'Sullivan MJ, Bond IP, Trask RS. Self-healing fibre reinforced composites via a bioinspired vasculature. Adv Funct Mater 2011;21:3624–33.
[24] Esser-Kahn AP, Thakre PR, Dong H, Patrick JF, Vlasko-Vlasov VK, Sottos NR, et al. Three-dimensional microvascular fiber-reinforced composites. Adv Mater 2011;23:3654–8.
[25] Dong H, Esser-Kahn AP, Thakre PR, Patrick JF, Sottos NR, White SR, et al. Chemical treatment of poly(lactic acid) fibers to enhance the rate of thermal depolymerization. Appl Mater Interf 2012;4:503–9.
[26] Nguyen DT, Kleinman M, Truong R, Esser-Kahn AP. Bio-inspired microvascular exchangers employing circular packing – synthetic rete mirabile. Mater Horizons 2014;1:602–7.
[27] Kleiman M, Brubaker KS, Nguyen DT, Esser-Kahn AP. Bio-inspired morphogenesis using microvascular networks and reaction–diffusion. Chem Mater 2015;27(13):4871–6.
[28] Gergely RCR, Pety SJ, Krull BP, Patrick JF, Doan TQ, Coppola AM, et al. Multidimensional vascular polymers using degradable sacrificial templates. Adv Funct Mater 2015;25:1043–52.
[29] Guo SZ, Gosselin F, Guerin N, Lanouette AM, Heuzey MC, Therriault D. Solvent-cast three-dimensional printing of multifunctional microsystems. Small 2013;9(24):4118–22.
[30] Patrick JF, Hart KR, Krull BP, Diesendruck CE, Moore JS, White SR, et al. Continuous self-healing life cycle in vascularized structural composites. Adv Mater 2014;26:4302–8.
[31] Gladman SA, Matsumoto EA, Nuzzo RG, Mahadevan L, Lewis JA. Biomimetic 4D printing. Nat Mater 2016;15(4):413–8.
[32] Katifori E, Szöllősi GJ, Magnasco MO. Damage and fluctuations induce loops in optimal transport networks. Phys Rev Lett 2010;104:1–4.
[33] Södergård A, Stolt M. Properties of lactic acid based polymers and their correlation with composition. Prog Polym Sci 2002;27:1123–63.
[34] Ingeo™ Biopolymer 4043D technical data sheet. NatureWorks, LLC, 15305 Minnetonka Boulevard, Minnetonka, MN 55345, USA; 2013.
[35] Cava D, Gavara R, Lagarón JM, Voelkel A. Surface characterization of poly(lactic acid) and polycaprolactone by inverse gas chromatography. J Chromatogr A 2007;1148:86–91.
[36] Cicero JA, Dorgan JR, Dec SF, Knauss DM. Phosphite stabilization effects on two-step melt-spun fibers of polylactide. Polym Degrad Stab 2002;78:95–105.
[37] Henton DE, Gruber P, Lunt J, Randall J. Polylactic acid technology. In: Mohanty A, Misra M, Drzal L, editors. Natural fibers, biopolymers, and biocomposites. Boca Raton, FL, USA: CRC Press Taylor & Francis Group; 2005. p. 527–77 [chap. 16].
[38] ASTM D3822: Standard test method for tensile properties of single textile fibers. ASTM International; 2007.
[39] Bogdanovich AE, Bradford P, Mungalov D, Fang S, Zhang M, Baughman RH, et al. Fabrication and mechanical characterization of carbon nanotube yarns, 3-D braids, and their composites. SAMPE J 2007;43(1):2–15.
[40] Bogdanovich AE, Mohamed MH. Three-dimensional reinforcements for composites. SAMPE J 2009;45(6):2–20.
[41] ASTM E1356: Standard test method for assignment of the glass transition temperatures by differential scanning calorimetry. ASTM International; 2008.
[42] Olson JR. System, apparatus, and method for micro-capillary heat exchanger. US Patent Publication No. 2013/0306279; 2013.
[43] Coppola A, Thakre P, Sottos N, White S. Tensile properties and damage evolution in vascular 3D woven glass/epoxy composites. Compos Part A: Appl Sci Manuf 2014;59:9–17.
[44] Coppola A, Griffin A, Sottos N, White S. Retention of mechanical performance of polymer matrix composites above the glass transition temperature by vascular cooling. Compos Part A: Appl Sci Manuf 2015;78:412–23.
[45] Pety SJ. Microvascular composites as a multifunctional material for electric vehicles. Ph.D. thesis, University of Illinois at Urbana-Champaign; 2017.
[46] Munson BR, Young DF, Okiishi TH. Fundamentals of fluid mechanics. 4th ed. New York, NY, USA: John Wiley and Sons; 2002.
[47] Patrick JF, White SR, Sottos NR, Moore JS, Krull BP. Advanced thermal processing techniques of "sacrificial" polylactic acid (PLA). US Patent Publication No. 2015/0137416; 2015.